NASA-CR-203697

MD-Vol. 43/AMD-Vol. 168, Material Parameter Estimation
for Modern Constitutive Equations
ASME 1993

A ROBUST METHODOLOGY FOR ESTIMATING MATERIAL PARAMETERS FOR THE RAMASWAMY-STOUFFER CONSTITUTIVE MODEL

James A. Sherwood and Richard J. Doore
Department of Mechanical Engineering
University of New Hampshire
Durham, New Hampshire

Abstract

The program MATS was developed in a previous study (Doore and Sherwood, 1993) to find material constants for the Ramaswamy-Stouffer constitutive model (Ramaswamy et al., 1990). The constants were used in that study to run simulations of Timetal-21s which were then compared to experimental results. In this study, parametric studies were performed to investigate the sensitivities of the material constants with respect to the others and the influence of the scheme for interpolating material constants for temperatures between known values in yielding a calculated response. The results of the parametric studies were used to "fine tune" the material constants and help determine the "best" interpolation scheme for capturing the transition from strain-rate-independent to strain-rate-dependent behavior.

Introduction

The Ramaswamy-Stouffer constitutive theory is a derivation of the Bodner-Partom model (1975). Both of these of constitutive theories are very capable of capturing thermomechanical behavior. However, the task of finding the required material constants can be convoluted and very time consuming. Several studies (Stouffer and Bodner, 1982; Ramaswamy, 1985; Sherwood, 1987; Chan et al., 1988; Sherwood and Fay, 1992) have addressed methodologies for determining the required material constants. However, there has not been a comprehensive

publication addressing the interaction of the constants in calculating a response. The scope of this paper is to address this void.

The Constitutive Model

The Ramaswamy-Stouffer constitutive theory is a temperature-dependant viscoplastic theory which has been incorporated into the ADINA (1987) finite element package by Sherwood and Boyle (1991). Material constants are derived from experimental testing of monolithic materials for use in the code. The state variables Z and Ω_{ij} represent changes in the microstructure and describe the isotropic and kinematic hardening contributions, respectively. The following equations summarize the constitutive theory.

The flow rule which has been modified by Sherwood and Stouffer (1992) to include an isotropic damage, ω, term is represented by,

$$\dot{\varepsilon}^I_{ij} = D_0 \exp\left(-\frac{1}{2}\left(\frac{Z^2(1-\omega)^2}{3K_2}\right)^n\right)\frac{S_{ij}-\Omega_{ij}}{\sqrt{3\bar{K}_2}} \tag{1}$$

where K_2 is analogous to J_2 and is given by

$$K_2 = \frac{1}{2}(S_{ij}-\Omega_{ij})(S_{ij}-\Omega_{ij}) \tag{2}$$

with the back-stress-evolution equation,

$$\dot{\Omega}_{ij} = \dot{\Omega}^E_{ij}+\dot{\Omega}^I_{ij} \tag{3}$$

expressed in terms of the elastic component,

$$\dot{\Omega}^E_{ij} = f_3 S_{ij} \tag{4}$$

and the inelastic component,

$$\dot{\Omega}^I_{ij} = f_1\dot{\varepsilon}^I_{ij} - \frac{2}{3}f_1\frac{\Omega_{ij}}{\Omega_s}\sqrt{\frac{2}{3}\dot{\varepsilon}^I_{ij}\dot{\varepsilon}^I_{ij}} \tag{5}$$

The back-stress-recovery equation is,

$$\dot{\Omega}_s = -B\left(\frac{\sqrt{3J_2}}{\sigma_o}\right)^r(\Omega_s-\Omega_{CRP}) \tag{6}$$

The drag-stress evolution is described by

The value of D_o is typically assumed to be 10^4 and is temperature independent. The remaining material constants n, f_1, f_3, B, r, m, and Z_1 are temperature dependent.

The Material

Timetal-21s was developed by TIMET, Henderson Technical Laboratory, Henderson, NV to be roughly equivalent to Ti-15V-3Cr-3Sn-3Al (Ti-15-3) in terms of processing and properties with the exception of significantly improved oxidation resistance. The exact fabrication process and chemical composition are proprietary and can not be included here. The initial application of Timetal-21s was as a matrix in a metal-matrix-composite structure which would be exposed to temperatures up to 815°C. The standard heat treatment for Timetal-21s is for eight hours at 621°C in a vacuum. The alloy is strip producible (low-cost foil), age hardenable and oxidation resistant (no vanadium).

Material Constants

The material constants for Timetal-21s were determined using the program MATS in a previous study (Doore and Sherwood, 1993). The values of the secant coefficient of thermal expansion (CTE) and Poisson's ratio, ν were supplied by the Materials Directorate of Wright-Patterson AFB, OH. Table 1 summarizes the material constants found in the previous study.

Table 1. Material Constants Calculated from Tensile Tests

Temp °C	Ω_{sat} MPa	Z_o MPa	n	E MPa	f_1	f_3
23	744	339	1.950	114290	44988	0.8795
260	573	382	1.850	108038	37002	0.8152
482	512	498	1.500	90374	35589	0.7954
650	55	1.24×10^{10}	0.100	74539	20500	0.1045
760	3	2.47×10^{8}	0.120	60278	990	0.0024
815	1	2.45×10^{8}	0.116	53224	760	0.0019

Experimental Data

The data used for the tensile tests were supplied by two sources. NASA-LeRC supplied the data for the tests at 23 and 482°C, and UDRI supplied the data used for 260 and 815°C. No tensile data were available at 650 and 760°C. The data used for 650 and 760°C are the first quarter cycle of the UDRI cyclic tests run at these temperatures. Single-step creep tests at two different stress levels were available at 650°C from NASA-LeRC. The filenames and the associated strain rates for the tensile and cyclic tests are listed in Table 2.

Table 2. Data Files for Timetal-21s

Filename	Temperature, °C	Strain Rate, s^{-1}
M04-3-1	23	8.33×10^{-5}
91-151	260	7.22×10^{-4}
91-152	260	1.87×10^{-5}
M04-3-11	482	8.33×10^{-5}
91-534	650	8.33×10^{-4}
91-533	650	8.33×10^{-5}
91-532	760	8.33×10^{-4}
91-530	760	8.33×10^{-5}
91-172	815	3.25×10^{-3}
91-173	815	3.25×10^{-3}

Parametric Studies

Parametric studies were conducted to determine the sensitivity of the calculated response to variations in the material constants. To interpolate the material constants at any temperature other than the six known temperatures, one must determine an interpolation scheme to generate constants that will predict reasonably accurate stress-strain curves. Also, due to experimental error and/or scatter, the program MATS does not always determine the "best fit". Therefore, it is sometimes necessary to manually tune the constants to obtain a "best fit". An understanding of how a material constant affects the stress-strain curve is needed to make these adjustments.

Interpolation of Material Constants

The simulation program does a linear interpolation to calculate material constants at intermediate temperatures where material tests are not available. This interpolation scheme assumes that the constants vary linearly between the two known temperatures. Simulations for Timetal-21s were conducted at temperatures halfway between all adjacent temperatures where data were available to investigate the consequences of this linear variation. The simulations produced reasonable results below 482°C where the tests were not strain-rate dependent. During the transition stage from strain-rate-independent to strain-rate-dependent behavior, i.e. 482 to 650°C and on through 760°C, the saturated stress levels at these halfway temperature points became unreasonably high. In contrast, the simulations between 760 and 815°C yielded reasonable results. Figure 1 shows the intermediate stress-strain curve at 142°C. All constants were linearly interpolated between 482 and 650°C. The constants at 566°C were entered into the rearranged form of the inelastic-flow equation at saturation as given by

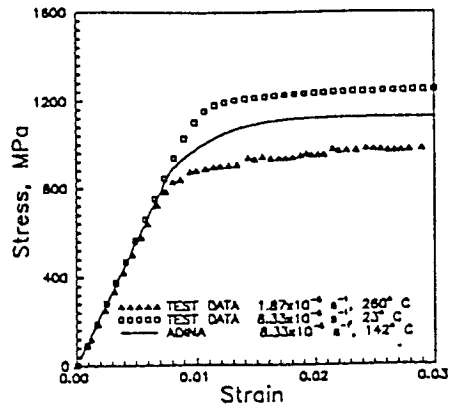

Figure 1 Comparison of the calculated response at 142°C with test data at 23 and 260°C

$$\sigma_{sat} = \frac{3}{2}\Omega_{sat} + \left[Z \left[-2\ln\left(\frac{\dot{\varepsilon}^I}{D_o} \frac{\sqrt{3}}{2} \right) \right]^{-\frac{1}{2n}} \right] \qquad (8)$$

at a strain rate of 8.33×10^{-4} s^{-1}, and the saturated-stress level, σ_{sat} was 14.78×10^{6} MPa. Eq. (8) assumes $\omega=0$, i.e. no damage. This extremely high σ_{sat} is approximately 4×10^{4} times greater than the expected range. Other calculations were made between 482 and 650°C, and similar results were observed. These high saturation levels occur in the transition region between the rate-independent and the rate-dependent temperatures. Unreasonably high saturated-stress levels were also occurring between 650 and 760°C. The transition between the strain-rate-independent and the strain-rate-dependent response is one area that needed to be better understood. The drag stress state variable, Z corresponds to the isotropic hardening (or softening) of the material. The drag stress controls the height of the hysteresis

loop by dictating the saturated-stress level. Because the Z_o value for Timetal-21s had an eight orders of magnitude increase from 482 to 650°C, the interpolation of the Z_o value was studied to conclude its influence on σ_{sat}. The equation for inelastic flow was rewritten to backsolve for the initial drag stress as

$$Z_o = \left(\sigma - \frac{3}{2}\Omega\right)\left[-2\ln\left(\frac{\sqrt{3}\,\dot{\varepsilon}^I}{2D_o}\right)\right]^{\frac{1}{2n}} \qquad (9)$$

where $\omega=0$. Eq. (9) was entered into a spreadsheet, and the values for n, f_1, f_3, and Ω were linearly interpolated between 482 and 650°C. The stress at 482°C was 917 MPa for strain rates of 8.33×10^{-4} and 8.33×10^{-5} s^{-1}. The stress at 650°C was 382 MPa for 8.33×10^{-4} s^{-1} and was 236 MPa for 8.33×10^{-5} s^{-1}. The saturated stress levels for both strain rates were assumed to vary linearly with respect to temperature between the 482 and 650°C. Using Eq. (9), the Z_o required to achieve the interpolated σ_{sat} was calculated for both strain rates. The back calculated values of Z_o for the two strain rates matched at their respective temperature points as expected. However, there was some difference between the two back calculated Z_o's for the respective strain rates at temperature points in the transition region. The values of Z_o at the two different strain rates were averaged at each temperature to yield a single value. The averaged Z_o value was used to calculate the two stress saturation curves between 482 and 650°C. The drag stress, Z_o was observed to vary exponentially as a function of temperature, not linearly as had previously been used. A plot of the σ_{sat} levels and ln Z_o versus temperature is shown in Fig. 2.

To capture the exponential growth of Z_o, two methods to make a smooth transition were implemented. Since Z_o grows exponentially with temperature, the interpolation scheme for Z_o was changed from linear to logarithmic. Tensile tests were simulated at the intermediate temperatures for the 23-to-482°C and 760-to-815°C temperature ranges. There was little difference between the calculated responses (less than 1 MPa) for a specific temperature in both regions when using either the

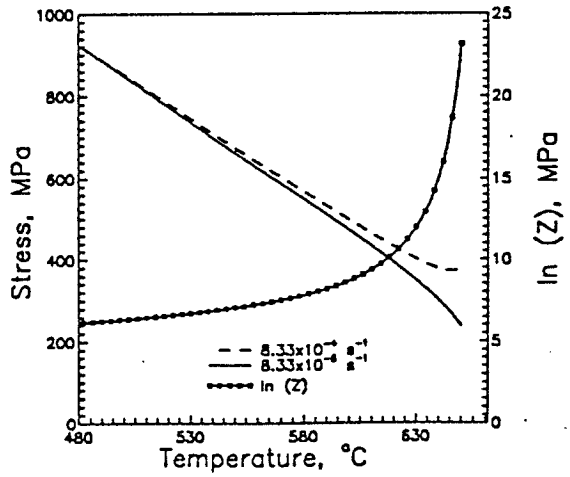

Figure 2 Calculated value of the drag stress compared to the interpolated stress levels during the transition stage

linear or logarithmic interpolation. However, in the temperature range from 650 to 760°C, the logarithmic interpolation removed the problem of unreasonably high saturated-stress levels. Fig. 3 shows the calculated stress-strain curve at 705°C as compared to the experimental data at 650 and 760°C. While this calculated response is not experimentally verified, it does appear to be reasonable.

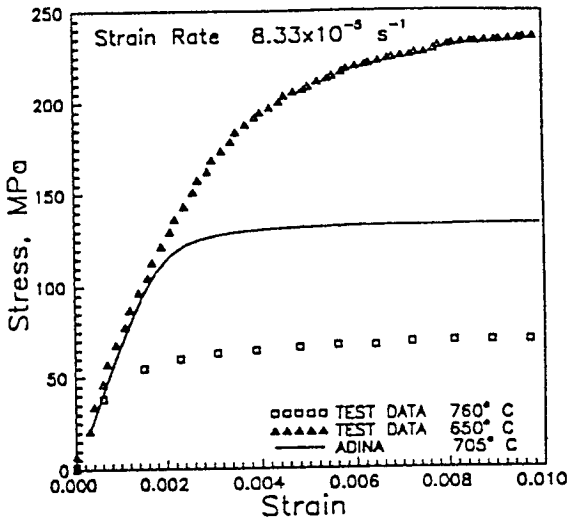

Figure 3 Comparison of the calculated response at 705°C with test data at 650 and 760°C

At 566°C, the midpoint of the transition stage, the saturated stress as calculated by the simulation using logarithmic versus linear interpolation was reduced by three orders of magnitude. However, this reduced value was still well above a reasonable one. The values for Z_o had been calculated for the transition from rate-independent to rate-dependent behavior assuming a linear dependence of saturated-stress level with respect to temperature. Intermediate sets of material constants were added at five temperatures between 650 and 760°C in an effort to improve the calculated stress response in this transition region. The material constants were back calculated using the data obtained from Fig. 2. The piecewise linear interpolation of the logarithm of Z_o and the resulting saturated-stress level are shown in Fig. 4. The saturated-stress levels between 600 and 650°C were still not reasonable, so five more temperatures were added to the material constant library to help smooth σ_{sat} in the transition region. A plot of the transition region σ_{sat}'s with ten intermediate steps is shown in Fig. 5. Figs. 6, 7 and 8 show how the material constants n, Z_o and Ω_{sat}, respectively, vary over the entire

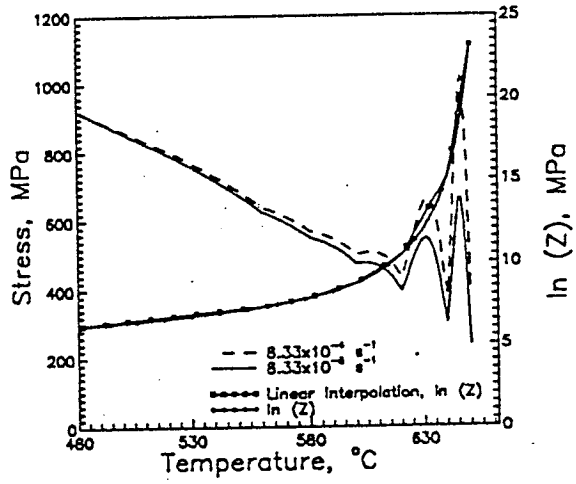

Figure 4 Five-step piecewise linear interpolation of the logarithm of drag stress compared to the calculated saturated-stress response

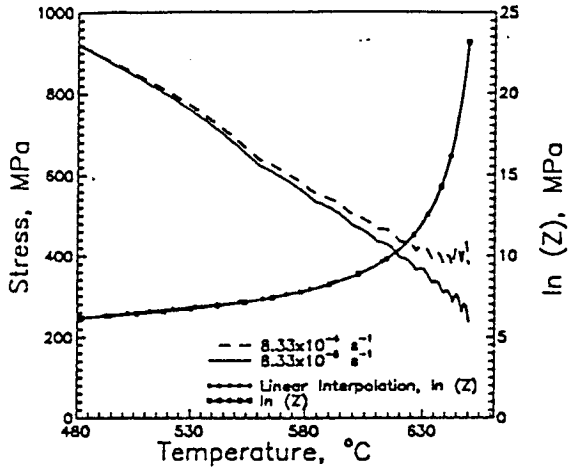

Figure 5 Ten-step piecewise linear interpolation of the natural logarithm of drag stress compared to the calculated saturated-stress response

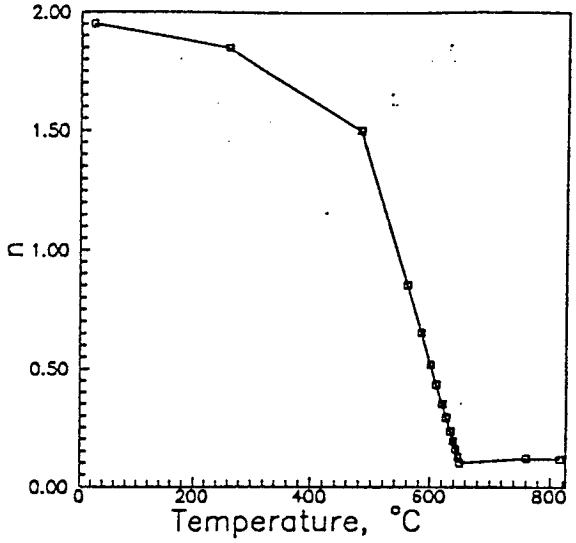

Figure 6 Variation of n as a function of Temperature

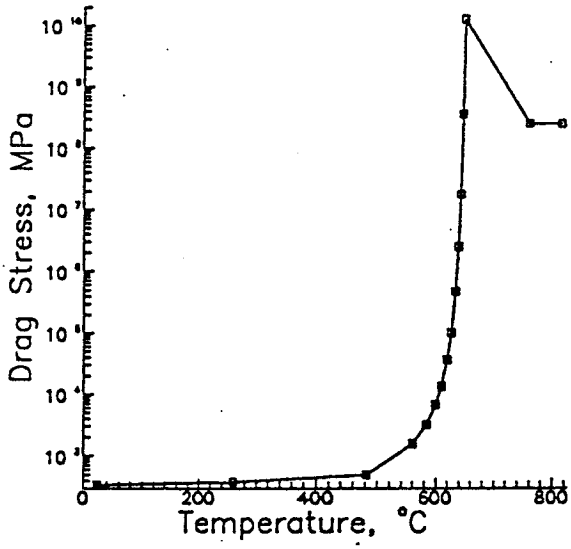

Figure 7 Variation of drag stress as a function of temperature

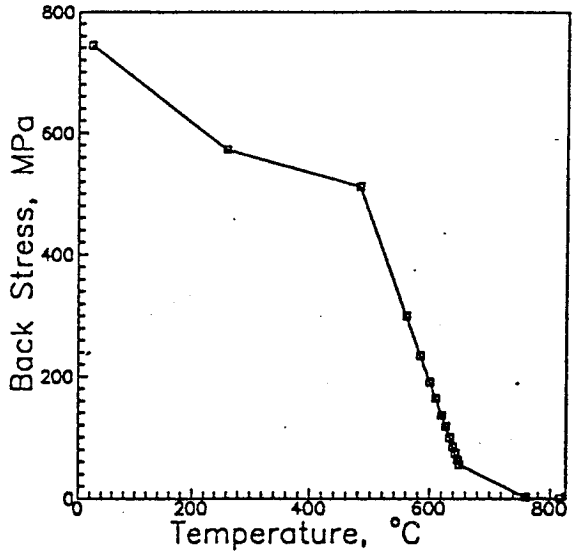

Figure 8 Variation of back stress as a function of temperature

temperature range. A plot of the saturated-stress level over the entire temperature range is given in Fig. 9. and shows the strain-rate dependence of the response.

The values for f_1, f_3 and E help define the shape of the stress-strain curve simulation. These values were linearly interpolated between the available adjacent temperature points and are shown in Figs. 10, 11 and 12. Fig. 13 shows a plot of a simulated tensile response at 566°C for a strain rate of 8.33×10^{-5} s^{-1} as compared with tensile data at 482 and 650°C for 8.33×10^{-5} s^{-1}. Fig. 13 shows that

the transition between strain-rate-independent and strain-rate-dependent saturated stress levels follows a logical course. Also, the material constants that help define the shape of the tensile curve are qualitatively validated at this intermediate temperature.

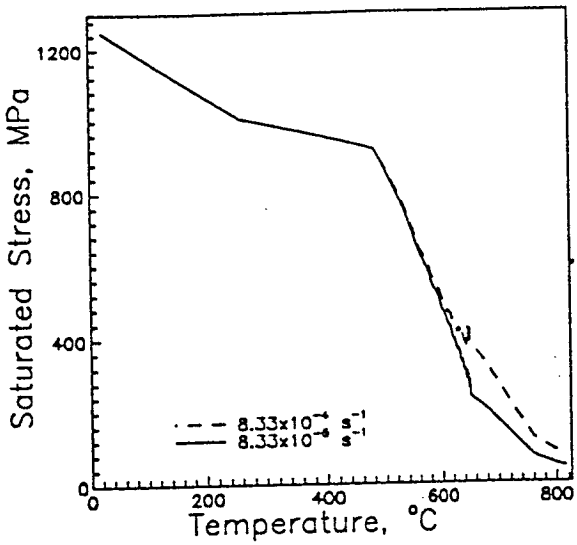

Figure 9 Variation of stress at two strain rates as a function of temperature

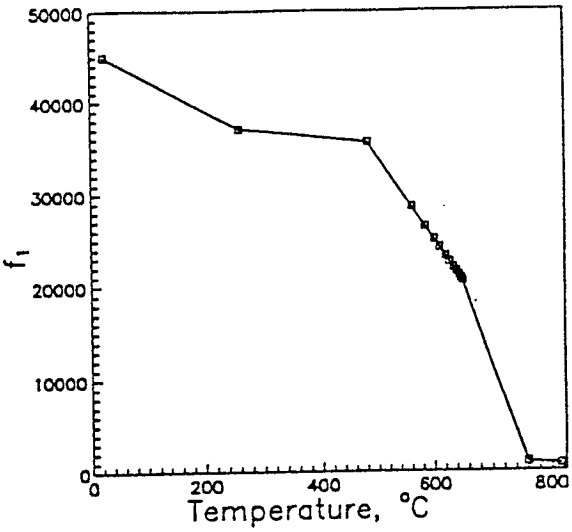

Figure 10 Variation of f_1 as a function of temperature

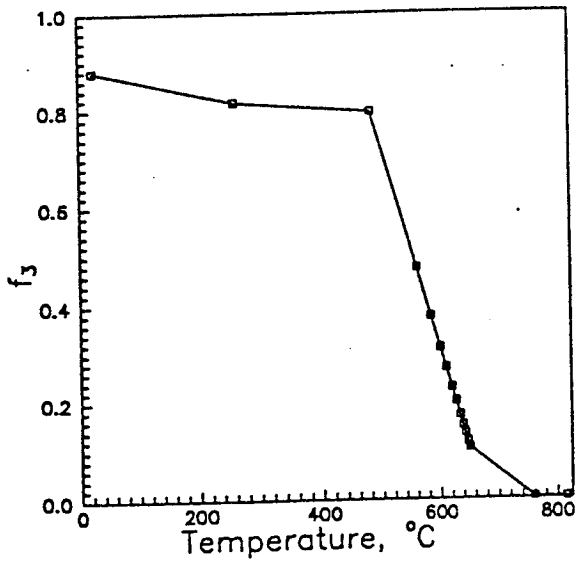

Figure 11 Variation of f_3 as a function of temperature

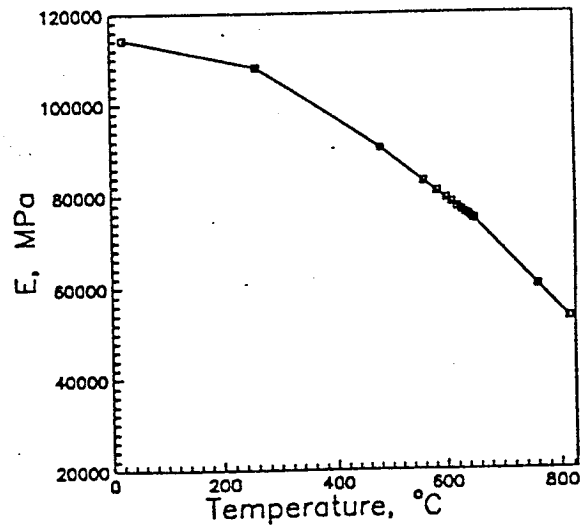

Figure 12 Variation of the modulus of elasticity as a function of temperature

Table 3. summarizes the material constants for the six temperatures at which data were available and the ten temperatures where material constants were added by the interpolation method described above.

Table 3. Material Constants (Calculated and Interpolated) from Tensile Tests

Temp °C	Ω_{sat} MPa	Z_o MPa	n	E MPa	f_1	f_3
23	744	339	1.950	114290	44988	0.8795
260	573	382	1.850	108038	37002	0.8152
482	512	498	1.500	90374	35589	0.7954
560	300	1565	0.850	83022	28583	0.4746
584	235	3173	0.650	80760	26428	0.3759
600	191	6684	0.517	79252	24991	0.3101
610	164	13256	0.433	78309	24093	0.2690
620	136	35973	0.350	77367	23194	0.2279
627	118	100730	0.292	76707	22566	0.1991
634	99	468069	0.233	76047	21937	0.1703
639	85	2471755	0.192	75576	21488	0.1497
643	74	17518370	0.158	75199	21129	0.1333
647	63	351869405	0.125	74822	20769	0.1168
650	55	1.24×10^{10}	0.100	74539	20500	0.1045
760	3	2.47×10^{8}	0.120	60278	990	0.0024
815	1	2.45×10^{8}	0.116	53224	760	0.0019

Sensitivities and Fine Tuning of the Material Constants

Sensitivity studies were conducted to gain an understanding of how changing a material constant affects the calculated stress-strain response. The main focus of this portion of the investigation was to gain an understanding of how the material constants affect the stress-saturation level during a tensile-test simulation. The sensitivities of the material

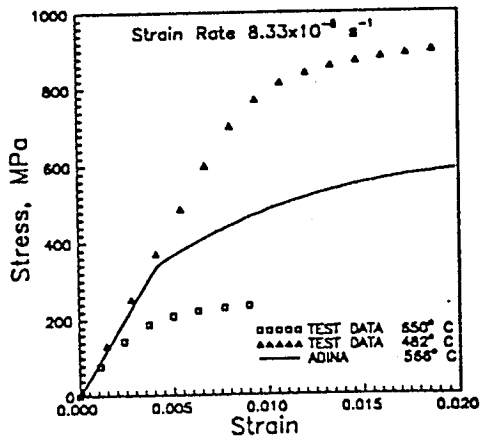

Figure 13 Comparison of the calculated response at 566°C with test data at 482 and 650°C

constants for the cyclic and creep simulations will be discussed at the end of this section.

From a material science viewpoint, the saturated-stress level is due to the presence of the back-stress and the drag-stress. The three constants that affect the saturated-stress level of a tensile-test simulation are the back stress, the drag stress and n. The back stress component that contributes to the saturated-stress level in a uniaxial tensile test is written as

$$\sigma_{sat} = \frac{3}{2}\Omega_{sat} \tag{10}$$

If the value of Ω_{sat} increases by one, the saturated-stress level will increase by 1.5. This relation is helpful when fine tuning a set of tensile-test simulations that all either undershoot or overshoot the experimental data by the same amount. The saturated back stress is the only constant that will change the stress-saturation level the same amount independent of strain rate.

The drag stress simulates the isotropic hardening. The drag stress and n work together to determine the saturated-stress level as a function of strain rate. Figure 14 shows the general shape of saturated-stress versus n at two strain rates for Z_o=1000 MPa and Ω_{sat}=500 MPa. The saturated-stress level starts at 1.5 times the back stress. Ignoring the back stress term, the saturated-stress level would be

$$\sigma_{sat} = Z\left[-2\ln\left(\frac{\dot{\varepsilon}^I\sqrt{3}}{D_0\ 2}\right)\right]^{-\frac{1}{2n}} \tag{11}$$

If the inelastic-strain rate and n are held constant, Z is directly proportional to the saturated-stress level. When n is greater than 0.4, the saturated-stress level becomes quite sensitive to any change in Z. This sensitivity means if n is anywhere greater than 0.4, an increase in Z will effect a significant increase in σ_{sat}.

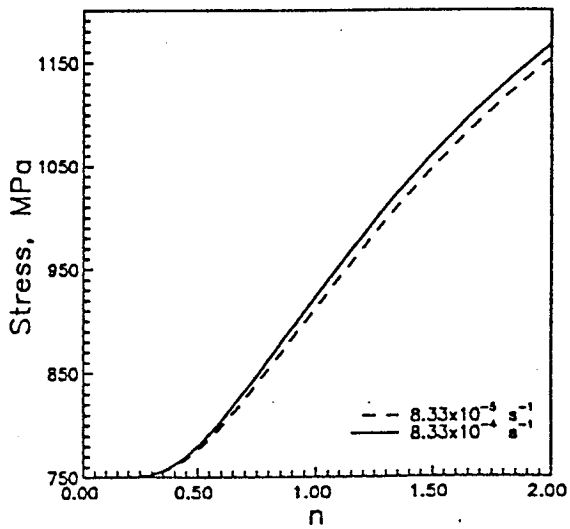

Figure 14 Variation of stress at two strain rates as a function of n

At this point, a deeper understanding of Eq. (11) is important when finding the material constants. Also, it is important to remember that the drag stress term will be added to the back stress term in Eq. (11). To get a σ_{sat}-level difference on the order of 100 MPa for strain rates in the range of 10^{-4} to 10^{-5} s^{-1} with an n from 0.4 to 2.0, Z has to be on the order of 10^5 MPa. The problem with this 10^5-MPa value for Z is that the σ_{sat} levels are consequently well above the 1000 MPa room-temperature σ_{sat} levels for the material considered in this study. As temperature increases, the strain-rate sensitivity typically increases, while the σ_{sat} level decreases. When n is small, there is very little difference in σ_{sat} levels as shown in Fig. 14. The only way to get a 100-MPa spread and keep the σ_{sat} levels within the desired area of interest is to let Z grow exponentially as n gets very small. Since the drag-stress term is added to the back-stress term to get the saturated-stress level, keeping the value of n small forces σ_{sat} levels for strain rates in the creep range to the correct level while letting stress levels associated with the higher strain rates to increase accordingly.

Ranges for Searching

When trying to find constants for a material, an understanding of where to pick search ranges for Z and Ω_{sat} is necessary. In the range where there is no strain-rate dependence, picking a start range for the back stress with an upper limit of 2/3 σ_{sat} has been found to be appropriate through numerical experiments. These same numerical experiments have shown that Z should start around 100. As the material starts to exhibit strain-rate dependence with increasing temperature, the upper limit on the start range for the back stress should be less than 2/3 the lowest σ_{sat} level--i.e. the σ_{sat} associated with the lowest available strain rate. At this point where strain-rate dependence is significant, n will need to become quite small and the Z search range will consequently have to be increased by orders of magnitude. The results from Timetal-21s are an excellent example of how the values of Z, n and Ω_{sat} change with increased strain-rate sensitivity.

After the constants Z, n and Ω_{sat} are calculated, the material constants controlling the shape of the stress-strain curve, specifically f_1, f_3 and E, are considered. When fine tuning a stress-strain curve to fit the "knee" of the data, these are the three constants used. The modulus of elasticity defines the slope of the curve. The value for f_3 relates Ω^E to the externally applied stress, σ, and the difference between σ and Ω dictates when inelastic flow

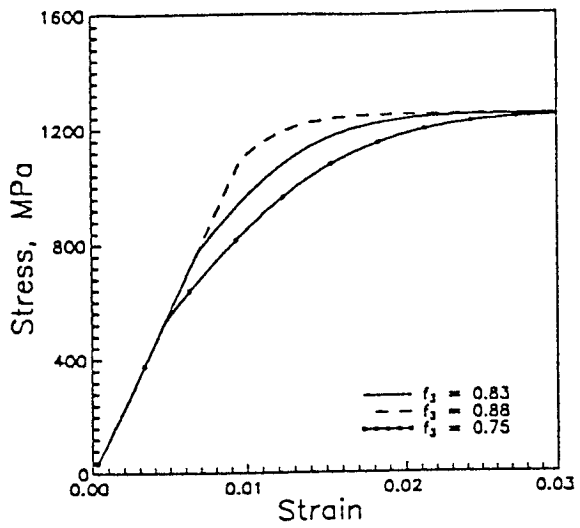

Figure 15 Sensitivity of the stress-strain curve to a change of f_3

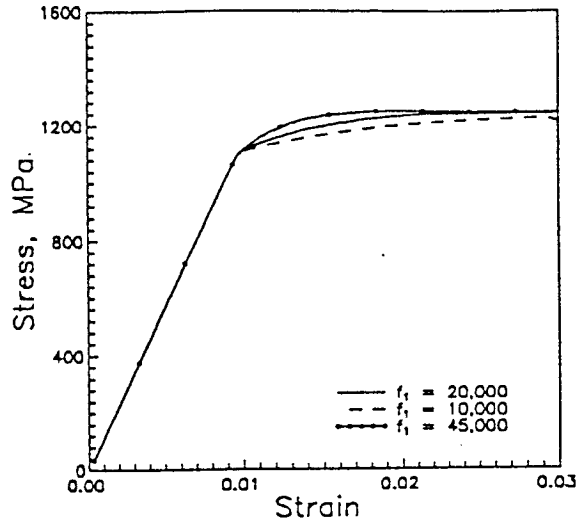

Figure 16 Sensitivity of the stress-strain curve to a change of f_1

initiates. If the calculated response initiates inelastic deformation at too low a strain value, f_3 can be raised, i.e. increase the elastic component of the back stress, to delay the initiation of inelastic flow. Fig. 15 shows how changing the value of f_3 influences the shape of the simulated curve at 23°C for Timetal-21s. The value of f_1 controls how fast the simulation achieves σ_{sat} after inelastic deformation begins. The value of f_1 is very insensitive to change at any temperature, and it is best to change f_1 in increments of 1000 when fine tuning the simulation. Fig. 16 shows how f_1 changes the stress-strain curve. At high temperatures where the saturated back stress becomes quite small, the simulated stress-strain curve is essentially insensitive to a change in either f_1 or f_3.

The material constants calculated from the cyclic tests are m and Z_1. The constants for this section of the material determination process did not need any fine tuning for Timetal-21s. Past experiences (Ramaswamy, 1985; Sherwood, 1987; Sherwood and Fay, 1992) for other materials have shown that the value for Z_1 generally does not need additional fine tuning. The only material constant that might need a small adjustment for this step in the material constant determination process might be m, the cyclic hardening or softening constant. If the simulation is not hardening at a high enough rate, adjustment of m in increments of 1% of m is recommended. The rate of cyclic hardening is directly proportional to m.

The constants for creep, B and r, are calculated using the time at saturation for a set of single-step creep tests. The method for calculating these constants is fairly accurate. Therefore, fine

tuning of the creep constants is generally not necessary. Thus, no recommendations are given here for the fine tuning of B or r.

Conclusions

Sensitivity studies were conducted to gain an understanding of how the material parameters must change to capture the effects of strain-rate sensitivity. These sensitivity studies can be used to guide in fine tuning the simulations to obtain a "best fit" to the experimental data. Some of the material constants change linearly while others vary exponentially with temperature. Appropriate interpolation schemes were implemented using this information. Using these interpolation schemes, the set of material constants found have the ability to capture the transition from stain-rate-independent to strain-rate-dependent behavior.

Acknowledgements

The authors wish to express their appreciation to Mike Castelli of NASA Lewis Research Center and Noel Ashbaugh and M. Khobaib of UDRI for providing the experimental data. Joe Klementovich of UNH helped greatly in the data reduction. This work was completed under NASA Grant NCC3-218.

References

ADINA, (1987), "A Finite Element Program for Automatic Dynamic Incremental Nonlinear Analysis," Report ARD 87-1, ADINA R&D, Inc., Watertown, MA.

Bodner, S.R. and Partom, Y., 1975, "Constitutive Equations for Elastic-Viscoplastic Strain-Hardening Materials," *ASME Journal of Applied Mechanics*, Vol. 42, pp. 385-389.

Chan, K. S., Bodner, S. R., and Lindholm, U. S., 1988, "Phenomenological Modeling of Hardening and Thermal Recovery in Metals," *ASME Journal of Engineering Materials and Technology*, Vol. 110, pp. 1-8.

Doore, R.J., and Sherwood, J.A., 1993, "MATS - An Automated Program for Finding Constitutive Model Constants," *ASME Journal of Engineering Materials and Technology*, (submitted for publication).

Ramaswamy, V.G., 1985, "A Constitutive Model for the Inelastic Multiaxial Cyclic Response of a Nickel Base Superalloy Rene 80," Ph.D. Thesis, University of Cincinnati.

Ramaswamy, V.G., Stouffer, D.C. and Laflen, J.H., 1990, "A Unified Constitutive Model for the Inelastic Uniaxial Response of René 80 at Temperatures between 538°C and 982°C," *ASME Journal of Engineering Materials and Technology*, Vol. 112, No. 3, pp. 280-286.

Sherwood, J.A., 1987, "A Constitutive Model with Damage for High-Temperature Superalloys," Ph.D. Thesis, University of Cincinnati.

Sherwood, J.A. and Boyle, M.J., 1991, "Investigation of the Thermomechanical Response of a Titanium Aluminide/Silicon Carbide Composite Using a Unified State Variable Model in ADINA," *Computers & Structures*, Vol. 40, No. 2, pp. 257-269.

Sherwood, J.A., and Fay, E.M., 1992, "Application of a Unified Constitutive Theory to the Nonproportional Multiaxial Strain Deformation of 1045 Steel," *ASME Journal of Engineering Materials and Technology*, Vol. 114, No. 2, pp. 147-155.

Sherwood, J.A., and Stouffer, D.C., 1992, "A Phenomenologically Based Constitutive Model with Damage for René 95," *ASME Journal of Engineering Materials and Technology*, Vol. 114, No. 4, pp. 340-347.

Stouffer, D.C., and Bodner, S.R., 1982, "A Relationship Between Theory and Experiment for a State Variable Constitutive Equation," ASTM STP 765, p. 239.